JOURNAL OF CATALYSIS 116, 540–555 (1989)

Monte Carlo Simulations of Supported Bimetallic Catalysts

JOHN K. STROHL AND TERRY S. KING

Department of Chemical Engineering, Iowa State University, 231 Sweeny Hall, Ames, Iowa 50011-2230

Received June 6, 1988; revised December 13, 1988

Supported bimetallic catalysts are modeled with a Monte Carlo simulation technique that uses a coordination-dependent potential model. Cubo-octahedral particles with dispersions ranging from 30 to 60% are studied as well as particles that have irregular shapes. Systems modeled include the Pt–Ib (Ib = Cu, Ag, Au), Ag–Ru, and Pt–Rh bimetallics. In the Pt–Ib systems, the Ib element segregates to the surface of the catalyst and tends to occupy the lowest coordinated sites first. Differences in the degree of surface segregation among the Ib elements are easily seen at higher Ib concentrations where Au is shown to segregate to the surface more strongly than Ag or Cu. The degree of clustering of Pt atoms on the surface of the catalyst particles depends on which Ib element is present. For a given amount of Ib atoms present on the surface the Au–Pt system is observed to produce larger ensembles of surface Pt atoms than the Ag–Pt or Cu–Pt systems. Predicted relative platinum dispersions for the Ag–Pt system were compared to hydrogen chemisorption measurements and found to be in good agreement except for one sample (30 wt% Ag) in which the measured value was found to be higher than the predicted value. This difference could be explained by a nonuniform distribution of silver in the catalyst sample or by the effect of chemisorption. In the Ag–Ru system, silver atoms are found to segregate to the surface and cluster together. Predicted relative ruthenium dispersion is compared to hydrogen chemisorption measurements and found to be in agreement. The Pt–Rh system showed that platinum atoms undergo net surface segregation, although rhodium atoms tended to dominate the corner and edge sites of the crystallites.

INTRODUCTION

Bimetallic catalysts have become the subject of increasingly intensive research efforts in both industrial and academic settings (*1–8*). Because of the myriad combinations possible, bimetallic catalysts have great potential to be tailored with respect to activity, selectivity, and stability. In the petroleum industry, for example, supported Pt reforming catalysts have been mostly replaced with supported Pt/Re or Pt/Ir or other platinum bimetallics that have superior activity and selectivity (*4*). On a more fundamental level, supported bimetallic catalysts are of interest from several points of view. Knowledge of surface composition and structure of bimetallic catalyst particles is certainly of primary importance not only in the characterization of the catalyst itself, but also in gaining insight into adsorption and catalytic reaction phenomena.

The small size of bimetallic catalyst particles (usually <100 Å) allows a relatively large fraction of metal atoms to be exposed on a surface and sometimes causes unexpected metal–metal interactions. For example, the Cu–Ru binary system exhibits immiscibility in bulk samples, yet experimental evidence suggests (*3*) that surprisingly strong interactions occur between these two metals in supported bimetallic catalysts. However, the small size of these bimetallic clusters—coupled with the fact that they are usually produced in a highly dispersed state on a support material such as alumina or silica in quantities less than 5 wt%—makes it difficult to determine experimentally the surface characteristics of the metallic particles.

Several theoretical approaches have been used to determine surface compositions of small bimetallic particles. Burton *et al.* (*9*) did not actually model small catalyst

0021-9517/89 $3.00

particles as such, but rather investigated multiatomic layered thin films by using regular solution theory, then extrapolated the results to make qualitative predictions regarding surface compositions of small spherical particles. The authors looked at ideal (Cu–Ni) and clustering (Au–Ni) systems and found that in the Cu–Ni system the copper segregated to the surface layer only, while in the clustering Au–Ni system the segregating component (Au) was also found in excess in several layers below the particle surface. Tsai *et al.* (*10*) assumed nearest-neighbor-only interactions and used Lennard–Jones potentials to model the metal–metal interactions in a Monte Carlo simulation that was applied to unsupported 55-atom clusters. Systems studied in this work included Cu–Ni, Cu–Ru, and Cu–Os. The researchers found surface enrichment of Cu in all cases, although the enrichment was greatest in the Cu–Ru and Cu–Os systems. A rigid lattice Monte Carlo procedure was used by Sundram and Wynblatt (*11*) on hypothetical, unsupported alloy particles in order to study segregation effects at low coordination sites. Fixed-morphology cubo-octahedral particles containing 38 and 201 atoms were simulated with both ordering and clustering alloys. The authors found that the degree of surface segregation to the lowest coordination sites on the particle surface was lower than that calculated for a thin film of equal overall composition because of competition by other surface sites for the segregating material.

In this paper we present results of Monte Carlo simulations of Pt–Ib (Ib = Cu, Ag, Au), Ag–Ru, and Pt–Rh bimetallic catalyst particles. The Monte Carlo method used in this research differs from those used previously in that a semiempirical pair potential is used that allows for metal–metal bond strengths to vary with coordination. Estimates of metal–support interactions are also taken into account in the simulations, and some simulations were performed without an assumption regarding initial particle shape. Overall surface compositions predicted for the Ag–Ru and Ag–Pt systems are compared to values obtained from hydrogen chemisorption experiments.

THEORY

The Monte Carlo method is a statistical sampling technique that, when applied to canonical systems, allows one to estimate certain macroscopic thermodynamic quantities (such as internal energy) by simple arithmetic averaging of a series of specially generated configurations of the system of interest. The first application of the Monte Carlo method to the solution of a physical problem was by Metropolis *et al.* in 1953 (*12*). Since that time the Monte Carlo method has been applied to an increasingly wide variety of problems in physics, chemistry, and engineering largely because of dramatic improvements in computer technology. Researchers in the areas of surface science and catalysis have made use of the Monte Carlo technique in describing surface segregation and composition of semi-infinite alloys (*11*, *13–15*).

In this work bimetallic catalyst particles were modeled by using the Monte Carlo method, initializing the atoms in an FCC lattice, and implementing the following algorithm:

1. An atom is selected and allowed to change positions in the lattice with either another atom or a vacancy.

2. The change in configurational energy ΔE, resulting from the switch described in step 1, is calculated.

3. If ΔE is negative, the new configuration is accepted. If ΔE is positive, a random number is selected from a uniform distribution. If the quantity $\exp(-\Delta E/kT)$ is greater than this random number, the new configuration is accepted; otherwise the old configuration is retained.

4. Steps 1–3 are repeated until "equilibrium" (no significant changes in total configurational energy occur with time) is reached. Dispersion averages and atomic

coordination statistics are gathered during the equilibrium period. (Because this atom-vacancy switching is allowed, particle morphologies as well as surface segregation effects can be computed.)

In these simulations an empirical potential model was used that allowed for the atom–atom bond energies to vary with coordination to better reflect actual behavior. This model, called the surface-modified pair potential model (SMPP), has been described in detail elsewhere (*13, 14*); therefore, only a brief discussion of its main features will be given below.

In any model of surface segregation, it is very important that the bond energies in the surface region accurately reflect the properties of a real alloy surface. One method of estimating bond energies as a function of coordination was developed by Schwoebel (*16*); it was later modified so it could be used in Monte Carlo simulation procedures of low index planes (*13, 14*). It is assumed that only nearest-neighbor interactions are considered and that the pairwise interaction energies vary with coordination of the two atoms that form the pair. It is also assumed that the total configurational energy of an atom is equally distributed among its nearest-neighbor bonds. Consider a single atom of species i of coordination n. Let ε_n^i be the contribution of this atom to the energy of the pairwise interaction with a nearest-neighbor atom of species i and coordination m. The energy associated with the pairwise interaction between these two atoms is then $\varepsilon_n^i + \varepsilon_m^i$. We now assume that ε_n^i can be represented by the empirical expression

$$\varepsilon_n^i = a^i + b^i n + c^i n^2, \qquad (2)$$

where a^i, b^i, and c^i are adjustable constants that can be determined from experimental data. We call ε_n^i the partial bond energy of i.

The constants a, b, and c are determined empirically from the heat of sublimation, ΔH_{sub}^i; the energy of bulk vacancy for motion, E_v^i; and the surface energy (not free energy or surface tension), σ_0^i by the relationships (*13*)

$$\frac{\Delta H_{\text{sub}}^i}{N_{\text{AV}}} = -12\varepsilon_{12}^i \qquad (2)$$

$$E_v^i = 12(11\varepsilon_{11}^i - 12\varepsilon_{12}^i) \qquad (3)$$

$$\sigma_0^i(100)\frac{a_0^2}{2} = 8\varepsilon_8^i - 12\varepsilon_{12}^i, \qquad (4)$$

where N_{AV} is Avogadro's number and $\sigma_0^i(100)$ is the surface energy for the (100) surface.

Empirically determined values can be found for the heat of sublimation (*17*), the energy of bulk vacancy formation (*18*), and surface energies (*19, 20*). Hence the empirical constants a, b, and c can be found for a pure metal using Eqs. (2)–(4). It is felt that this empirical quadratic expression is flexible enough to model the unknown functionality of partial bond energy variation with coordination. Typical values for the constants are given in Table 1.

The simple, empirical approach described above demonstrates how bond energies vary with coordination of the atoms involved. For example, the lateral surface bonds for the metals listed in Table 1 are 14 to 17% stronger than the corresponding bulk bonds. The vertical bonds from the surface are 7 to 9% stronger.

In modeling allows we must make the further assumptions that i–i and j–j pair interactions in the alloy are given as above for the pure materials and that i–j pair interactions can be determined via a mixing model (*21, 22*). Ideal and regular solution

TABLE 1

Empirical Expression for the Surface-Modified Pair Potential $\varepsilon_n^A = a^A + b^A n + c^A n^2$

A	a^A(eV)	b^A(eV)	c^A(eV)
Ni	−0.5530	0.007794	0.0006268
Cu	−0.3925	−0.001112	0.0008078
Ag	−0.2397	−0.01601	0.001301
Au	−0.3049	−0.02587	0.002070
Pt	−0.4015	−0.05232	0.003759

models of a mixture require the solution to be configured randomly. The nonrandom approach is more accurate, in general, in that no assumptions regarding clustering or ordering are made. According to this approach, the molar excess free energy of mixing, ΔG^{ex}_{mix}, is (*22*)

$$\frac{\Delta G^{ex}_{mix}}{ZRT} = X_i X_j \frac{w_{ij}}{ZkT}\left(1 - X_i X_j \frac{w_{ij}}{ZkT}\right), \quad (5)$$

where W, the so-called interchange energy, is given as

$$w_{ij} \equiv Z\left[E_{ij} - \left(\varepsilon^i_n + \varepsilon^j_m\right)\right]. \quad (6)$$

In addition, Z is the coordination number for the bulk lattice, X_i and X_j are the respective mole fractions, and E_{ij} is the pair interaction energy for a bulk i–j pair. By definition, w_{ij} is invariant with composition. Collaterally, it is assumed that w_{ij}/Z is independent of the coordination of the participating pair atoms and is independent of temperature. Then E_{ij} between an i atom of coordination n and a j atom of coordination m is given by

$$E_{ij} = w_{ij}/Z + (\varepsilon^i_n + \varepsilon^j_m), \quad (7)$$

thereby accounting for the effect of coordination on an i–j pair interaction.

The above pairwise bond model adequately describes metal–metal bonds and metal/vacuum interfaces. Additional energy terms are needed to describe chemisorption (*14*) and metal/support interfaces. For example, the energy change associated with chemisorption must account for formation of the chemisorptive bond and for any concomitant metal–metal bond energy variations. For nondissociative chemisorption the modeling of the effects of chemisorption on the surface segregation behavior of the bimetallic particles is relatively straightforward. The heat of chemisorption on each surface atom is added to the configurational energies in the algorithm. Since in the Monte Carlo procedures only differences in energy are calculated, PV terms (differences between energy and enthalpy) cancel out as long as the stoichiometry of chemisorption is the same on each metal. A similar approach can be used for dissociative adsorption as long as the adsorbate chemisorb on both metals. Otherwise, there is uncertainty as to what the energetic effects of chemisorption will be. For the results presented in this work, site-specific and coverage-dependent heats of chemisorption were not used, although these effects could be incorporated if known.

The most significant feature of the surface-modified pair potential is that it gives empirical values of pairwise interactions that are a function of the coordination of the two atoms forming the pair. These pairwise interactions are easily calculated and used in the Monte Carlo procedure. For low-index planes this approach has been shown to be suitable (*14*). In the application to small particles the empirical expression for the configurational energy given by Eq. (1) is forced beyond the range of coordination (n) for which the empirical constants were determined (Eqs. (2)–(4)). This is unfortunate and a potential source of error in the simulations. This problem may be alleviated by use of empirical data on systems of low coordination such as diffusion of adatoms on low-index planes or surface phonon information for small particles. However, until these data become readily available the extrapolation is necessary. More detailed models of varying degrees of rigor of metal clusters are being developed. A number of researchers have described an "embedded atom method" (*23–27*). Also, detailed, total energy calculations have been used (*28–31*). The problem with these approaches is that computation time is substantially larger making parametric simulation of the type described here impossible. As techniques improve and computational power increases, this relative disadvantage of the more sophisticated approaches will diminish.

As stated above, the algorithm used in this work allows for the exchange of atoms with vacancies. To compute the configurational energy change that would occur for

such an exchange, one must not only be concerned with the configurational energy of the atom undergoing the change in the lattice position, but also with that of the nearest-neighbor atoms to both the atom and the vacancy sites. These nearest-neighbor atoms must be taken into consideration since they also experience a change in bond numbers and strengths.

Metal–support interactions were modeled by adding an additional energy term to atoms located adjacent to the support. The magnitude of this energy term was estimated from data obtained by Pilliar and Nutting for the Ib metals on α-Al_2O_3 (*32*). The value for Pt was taken to be the arithmetic average of the Ib values. The metal–support energetic values obtained from Ref. (*32*) are roughly 5 to 10 times less than typical configurational energy differences resulting from changes in metal–metal bonding as atoms are switched around. Thus, the metal–support energy terms tend to have negligible influence on surface composition and ensemble sizes.

METHODS

Procedure Used for the Pt–Ib Simulations

The crystallites modeled in this study were, for the most part, assumed to have a perfect cubo-octahedral structure with both (100) and (111) facets being present on the surface. This structure is reasonably assumed as being representative since variations of octahedral structures are commonly observed experimentally for supported catalysts whose metals exhibit an FCC structure in the bulk (*33, 34*). It should be noted, however, that other shapes have been observed experimentally for pure Pt and Pt-containing bimetallic catalysts (*35, 36*). The paper by Harris (*36*) provides an excellent discussion of the effect of catalyst preparation on particle morphology. However, regardless of the exact particle shape, there is general agreement that the low-index planes, such as the (111) and (100) planes, predominantly form the surfaces of reduced FCC metallic catalysts. Therefore, the trends observed on the cubo-octahedral particles regarding segregation to low-coordinated sites and ensembling effects should be generally applicable to other morphologies as well. The use of the cubo-octahedral crystal structure allowed for the straightforward examination of size effects as well as the effect of the different Ib metals on the occupation of surface locations by Pt atoms. Four sizes of cubo-octahedral crystallites with a (100) plane adjacent to the support were used in the simulations. The structures contained 201, 586, 1289, and 2406 atoms with corresponding dispersions (excluding the face adjacent to the support) of 60, 46, 37, and 31%, respectively. The size range of these particles was approximately 2 to 4.5 nm. Many of the simulations of the perfect cubo-octahedral crystallites were conducted at a temperature of 550 K, which is representative of the temperature at which these catalysts are used. An atom occupying a given lattice position was selected for a possible switch 50 times. Generally, after 35 selections equilibrium was reached and averaging was begun. Some simulations were conducted in which the atoms were initialized in a rectangular block formation and "heated" to a high temperature to increase the mobility of the atoms and allow them to seek an equilibrium structure. Subsequent cooling to the desired temperature resulted in some additional morphological changes and allowed the surface composition and ensemble sizes to reach an equilibrium state. The purpose of these studies was to determine whether such a technique could produce crystallite shapes consistent with experimentally observed shapes and to compare dispersions and nearest-neighbor data of these computer-generated shapes with those of the perfect structures. It should be emphasized that during the simulation of the cubo-octahedral particles no special means were used to force this structure to remain fixed; because of the stability of this morphology, however, no

change in shape was ever observed. In all simulations, regardless of the initial morphology of the particle, atoms were placed randomly in the lattice before the Monte Carlo procedure was started.

Procedure Used for Ag–Ru Simulations

Monte Carlo simulations were performed on supported 2406 atoms (31% dispersion), cubo-octahedral Ag–Ru particles in order to compare the relative ruthenium dispersions with those measured by hydrogen chemisorption. A rigid-lattice simulation for this system may not be strictly valid, because silver exhibits an FCC structure and ruthenium is HCP. However, since ensuing simulation results showed clearly that the silver atoms strongly segregated to the surface and became highly clustered, it was thought that approximating the entire particle as one crystal structure (FCC) would not significantly affect a quantity such as relative dispersion.

Procedure Used for Pt–Rh Simulations

Since some alloy catalysts of commercial importance contain platinum and rhodium atoms, several simulations were run of unsupported crystallites comprising these elements. A cubo-octahedral shape was again used, and the particles modeled contained 1289 atoms (37% total dispersion). Because surface free-energy data for solid rhodium were unavailable, an estimate was made from the surface tension of rhodium at the melting point (*20*). The heat of mixing for the Pt–Rh system, which was used for the determination of the interchange energy, was obtained from the estimate provided in Ref. (*37*).

EXPERIMENTAL

In order to see if the Monte Carlo simulations could accurately predict the relative dispersions of group VIII metals in bimetallic catalysts, hydrogen chemisorption experiments were performed on supported Ag–Pt and Ag–Ru catalysts. All catalysts were prepared by incipient wetness impregnation with a silica support (Cab-O-Sil HS5, 300 m^2/g surface area). Precursors used for the group VIII metals were $Ru(NO)(NO_3)_3$ (AESAR) and $Pt(NH_3)_4(NO_3)_2$ (Alfa), while $AgNO_3$ (AESAR) provided the source of silver. Approximately 2.3 ml of impregnating solution per gram of dried support was sufficient to bring about incipient wetness. The amount of ruthenium or platinum was maintained constant at 4 wt% on a basis of metals plus dry support while the amount of silver was varied. After impregnation, the catalysts were oven-dried for 4 hr at 383 K. The reduction of Ru and Ag–Ru catalysts was carried out under flowing hydrogen (about 100 cc/min) at 723 K for 2 hr. The Pt and Ag–Pt catalysts were calcined at 723 K in flowing air for 1 hr before being reduced in flowing hydrogen at 723 K for 2 hr.

Chemisorption was carried out on a standard BET/chemisorption apparatus. A catalyst sample was held in a spherical Pyrex cell connected to the sample port of the apparatus. The cell was heated to 573 K and the sample was reduced under static hydrogen at about 760 Torr and subsequently outgassed overnight. Hydrogen chemisorption was carried out at room temperature at a pressure range of about 0 to 50 Torr. An equilibration time of 4 hr was sufficient for the first dose; 1 hr sufficed for subsequent doses. A 15-min evacuation of the sample cell was performed between total and reversible (weak) chemisorption measurements. The irreversible (strong) uptake was obtained by taking the difference between the values of the total and reversible isotherms extrapolated to zero pressure. Dispersions were obtained by assuming a 1 : 1 stoichiometry between hydrogen and Ru or Pt atoms and no spillover of hydrogen to silver.

RESULTS AND DISCUSSION

Pt–Ib System

The data obtained from the cubo-octahedral particle simulations for the Pt–Ib system have been compiled and summarized to

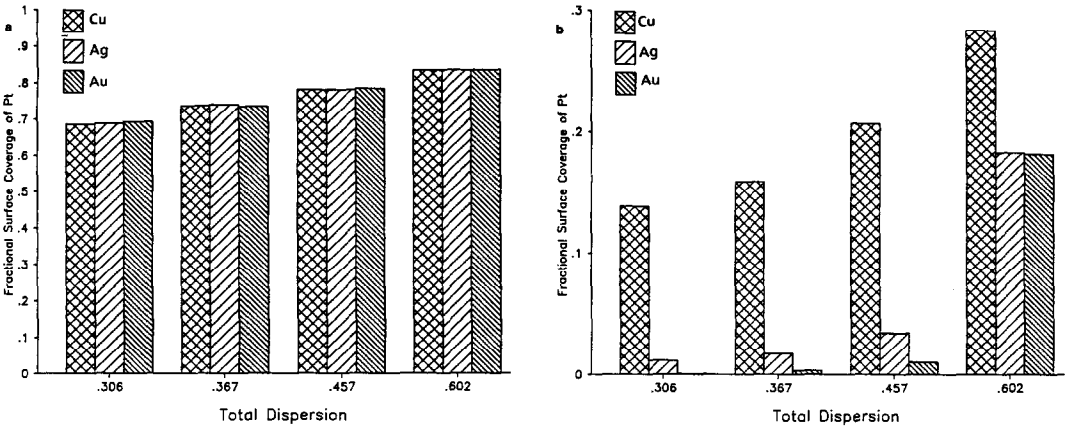

FIG. 1. Effect of Ib species on the fraction of platinum atoms on the surface of a bimetallic particle: (a) 10% Ib content, T = 550 K; (b) 50% Ib content, T = 550 K.

illustrate the overall surface composition of the particles, the surface location preferences of the different species, and the effect of the Ib metals on surface ensemble sizes of Pt atoms. Particle size effects will also be briefly discussed.

Figure 1 shows how the type and amount of Ib species present affects the surface composition (expressed as the fraction of surface atoms that are platinum) of the catalyst particle. Notice that in Fig. 1a, the overall surface composition for a particle with 10% Ib content is insensitive to which Ib species is present. However, when the Ib content is increased to 50% as shown in Fig. 1b, the surface composition is dramatically affected by which particular Ib metal is present. The reason this behavior occurs may be understood by studying Tables 2 and 3. Table 2 shows the change in configurational energy that would occur if a bulk (fully coordinated) Ib atom was to exchange places with a Pt atom on the surface of the particle. In each case, the configurational energy change is negative, which (neglecting other energy changes for the moment) implies that the Ib atoms prefer to be at the surface of the particle. Note also in Table 2 that the configurational energy driving force decreases within each Pt–Ib system as the coordination for the surface site increases. For example, the configurational energy change resulting from a bulk Ib atom switching with a 9-coordinated, surface Pt

TABLE 2

Configurational Energy Changes for Bulk Ib Atoms Switching with Surface Pt Atoms

Coordination of surface Pt atom	Configurational energy change (kJ/mole) for bulk Ib atom being switched		
	Au	Cu	Ag
6	−80.4	−108.4	−113.5
7	−63.4	−79.4	−82.4
8	−43.3	−52.6	−54.3
9	−26.1	−29.5	−30.7

TABLE 3

Mixing Energies for Pt–Ib Atom Pairs

Bond pair	Mixing energy[c] (w_{ij}/z)	
	eV/bond	kJ/mole
Au–Pt	0.0226[a]	2.2
Cu–Pt	−0.0336[a]	−3.2
Ag–Pt	0.0000[b]	0.0

[a] Determined from free energy of mixing data in Ref. (*38*).
[b] Obtained from estimate in Ref. (*37*).
[c] See Eq. (7).

atom is only one-third to one-fourth the configurational energy change observed when the switch occurs between a bulk Ib atom and a 6-coordinated Pt atom. Thus, there is a strong tendency for the Ib atoms, regardless of type, to first occupy the low-coordinated corner and edge atoms on the crystal surface. Once these low 6- and 7-coordinated sites have become populated with Ib atoms, however, the contribution to the total energy change by mixing energy becomes relatively greater. This is because of the aforementioned decrease in configurational energy change as Ib atoms go to the more highly coordinated surface sites and the fact that there are more nearest neighbors to interact with at these sites. In Table 3, which lists the mixing energy for each of the binaries, one can see that the Au–Pt system shows an endothermic heat of mixing, the Ag–Pt system shows a zero heat of mixing, and the Cu–Pt system shows an exothermic heat of mixing. These differences in heats of mixing in effect modulate the degree of surface segregation of the Ib species on the (111) facets. In the case of the Au–Pt system, the endothermic nature of the Au–Pt bonds tends to aid in repelling the Au atoms away from the core of fully coordinated Pt atoms and to the surface. On the other hand, Cu atoms, because of their exothermic bonding with Pt atoms, have less of an overall driving force for migrating to the surface of the particle.

Another phenomenon illustrated by Figs. 1 and 2 is the effect of particle size on over-

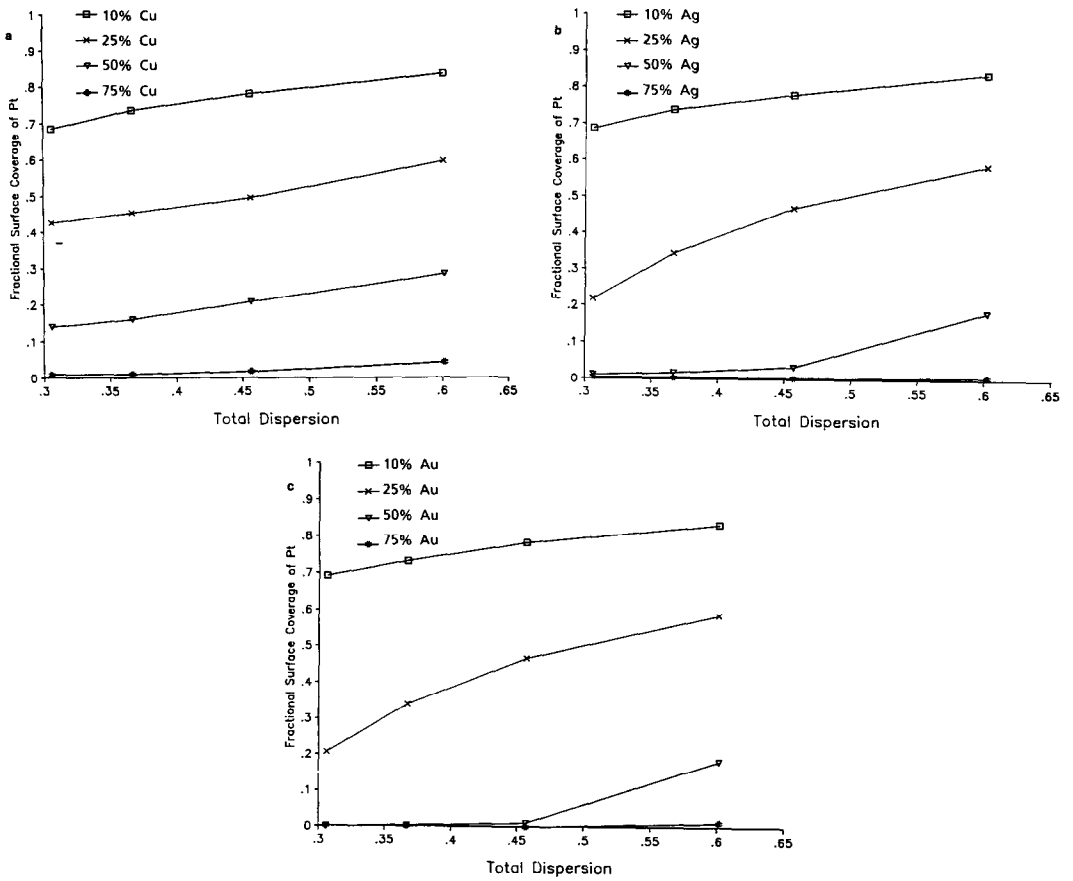

FIG. 2. Effect of particle size (dispersion) on overall platinum surface coverage in Pt–Ib particles: (a) Cu–Pt, T = 550 K; (b) Ag–Pt, T = 550 K; (c) Au–Pt, T = 550 K.

all Pt surface coverage. Each of these figures demonstrates that for a given overall Ib content the smaller, more highly dispersed particles have a greater proportion of Pt atoms in the surface. The reason for this behavior is that the larger particles have relatively fewer surface sites available for occupation by Ib atoms. Table 4 illustrates this surface/volume effect by listing the ratio of Ib atoms present in a 40% overall concentration to total surface atom sites for the four sizes of cubo-octahedral particles studied. Note that for the 201- and 586-atom particles the ratio of Ib atoms to surface atom sites is less than one. This means that even if all of the Ib atoms were to segregate to the surface of these particles, there would still be some Pt atoms present at the surface. On the other hand, the ratio of Ib atoms to the surface atom sites on the 1289- and 2406-atom particles is greater than one, indicating that the Ib atoms have the potential of blanketing the entire surface of the crystallite.

A comparison of predicted surface coverage of Pt in Ag–Pt bimetallic catalysts with chemisorption measurements is shown in Table 5. The degree of Pt surface coverage is given in terms of relative dispersion, that is, the ratio of the number of surface platinum atoms to the total number of platinum atoms. Note that agreement between measured and predicted relative platinum dispersion is very good in the catalysts with the lower silver content (5.8 to 20%); however, there is a difference in the predicted and measured values in the catalyst that contains 30% silver. One possible explanation for this discrepancy is that the Ag–Pt system actually has a negative heat of mixing rather than a zero heat of mixing (as estimated from Ref. (*37*)); this could result in the experimentally observed greater abundance (compared to the simulation results) of Pt atoms at the surface. Another possibility is that there is an uneven distribution of silver atoms between particles at this high silver concentration, even to the point of having nearly pure silver particles present. This latter explanation seems more likely, since the heat of mixing values required in the simulation to generate relative Pt dispersions close to that observed in the 30% silver particle is excessive (~90 kJ/mole).

Another reason for this discrepancy could be the effect hydrogen chemisorption has on the segregation behavior. If the difference in the heat of chemisorption on the two elements becomes comparable to configurational energy changes given in Table 2, then the effect of the configurational energy change can be wiped out by chemisorption. The problem with modeling chemisorption, however, is knowing the details of chemisorption. In the first place,

TABLE 4

Ratio of Ib Atoms to Number of Surface Sites Available on Perfect Cubo-octahedral Particles for 40% Ib Content

Size of particle (No. of atoms)	Dispersion	Ib/surface site ratio
201	0.602	0.664
586	0.457	0.875
1289	0.367	1.09
2406	0.306	1.31

TABLE 5

Comparison of Relative Pt Dispersions between Monte Carlo Predictions and Chemisorption Measurements

Atomic % Ag	$Pt^{Surface}/Pt^{Total}$			
	H_2 chemisorption	Monte Carlo[a]		
		0[b]	5[b]	10[b]
0.0	0.460	0.457	0.457	0.457
5.8	0.410	0.424	0.423	0.427
10.0	0.385	0.397	0.398	0.406
20.0	0.381	0.327	0.330	0.350
30.0	0.326	0.240	0.260	0.380

[a] 586-atom cubo-octahedral particle.
[b] Energetic effect of chemisorption of 0, 5, or 10 kcal/mole(Pt).

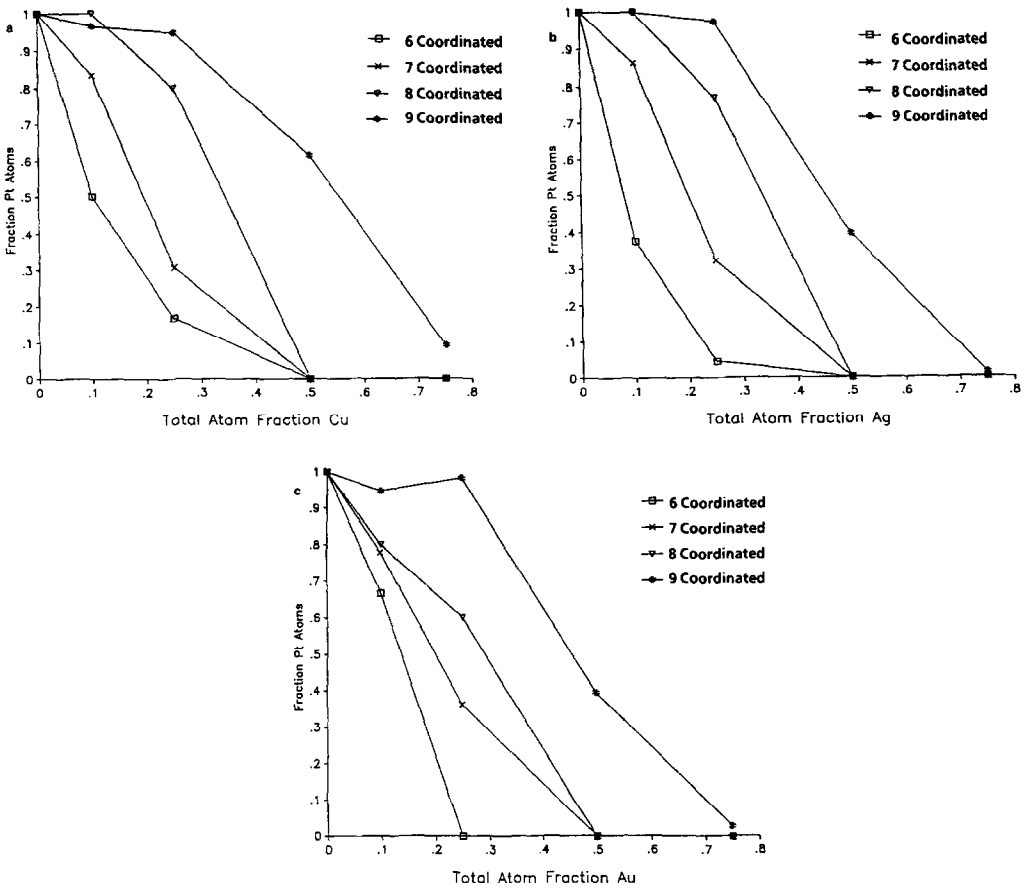

FIG. 3. Fraction of platinum atoms occupying sites on a 201-atom cubo-octahedral particle surface: (a) Cu–Pt, T = 550 K; (b) Ag–Pt, T = 550 K; (c) Au–Pt, T = 550 K.

the heats of chemisorption in general are not known with great accuracy. Also, the adsorption site and coverage dependence of the heat of adsorption can be important factors. In Table 5 the effect of chemisorption on the Monte Carlo results are presented. For the purposes of these calculations it was assumed that the difference in energy in the chemisorptive bond for silver–hydrogen and platinum–hydrogen was invariant with coverage and site. It is also assumed that the metal atoms are totally mobile so that equilibrium of segregation can be achieved.

Note that even relatively small variations in chemisorption energies between elements can have a significant effect on the predicted relative dispersion and surface composition for the higher silver content particles.

The preferential filling of the lower coordinated surface sites by the Ib atoms can be seen in Fig. 3 for the 201-atom particle. Note that in each case the surface Pt atoms become rapidly depleted from the 6-coordinated corner sites and 7-coordinated edge sites as increasing amounts of Ib atoms are added. In contrast, the 8-coordinated sites on the (100) planes and the 9-coordinated sites on the (111) planes show much less relative depletion of Pt as the Ib content is increased. The 9-coordinated sites are especially resistant to Pt depletion and continue to retain Pt atoms when the other sur-

face sites have become completely occupied by Ib atoms. This trend is what one would expect in looking at the configurational energy changes listed in Table 2. The Ib atoms have a relatively large configurational energy driving force segregating them in the 6- and 7-coordinated sites and a correspondingly smaller driving force "pushing" them toward the low-index planar sites.

The effect that the different Ib atoms have on the surface ensemble sizes can be readily seen by examining Fig. 4. This figure shows the predicted configurations of a series of 2406-atom (31% dispersion) particles with equal numbers of Ib atoms present at the surface. Note the dramatic difference between ensemble sizes of platinum atoms between the Cu–Pt and the Au–Pt crystallites. The copper atoms, because of their exothermic bonding nature with platinum atoms, tend to surround the platinum atoms, leaving them isolated either singly or in small groups. Conversely, the endothermic bonding nature of the Au–Pt pair results in the clustering of the platinum atoms into relatively large islands. The zero heating of mixing predicted for the Ag–Pt system results in the random distribution of ensemble sizes observed for this crystallite.

To illustrate further the variation in mixing behavior, Table 6 presents a tabulation of the Ib effects on Pt ensemble sizes for the particles shown in Fig. 4. The average number of surface Pt atoms that are nearest neighbors to a surface Pt atom is used as an indication of ensemble size. The greater the clustering tendency of the Pt atoms, the larger this number will be. Thus by looking at Table 6, one can see that there is a much greater inclination for the platinum to cluster when it is combined with gold than when combined with copper. In this instance, even though both crystallites contain the same overall surface concentration of platinum (25%), a platinum atom on the

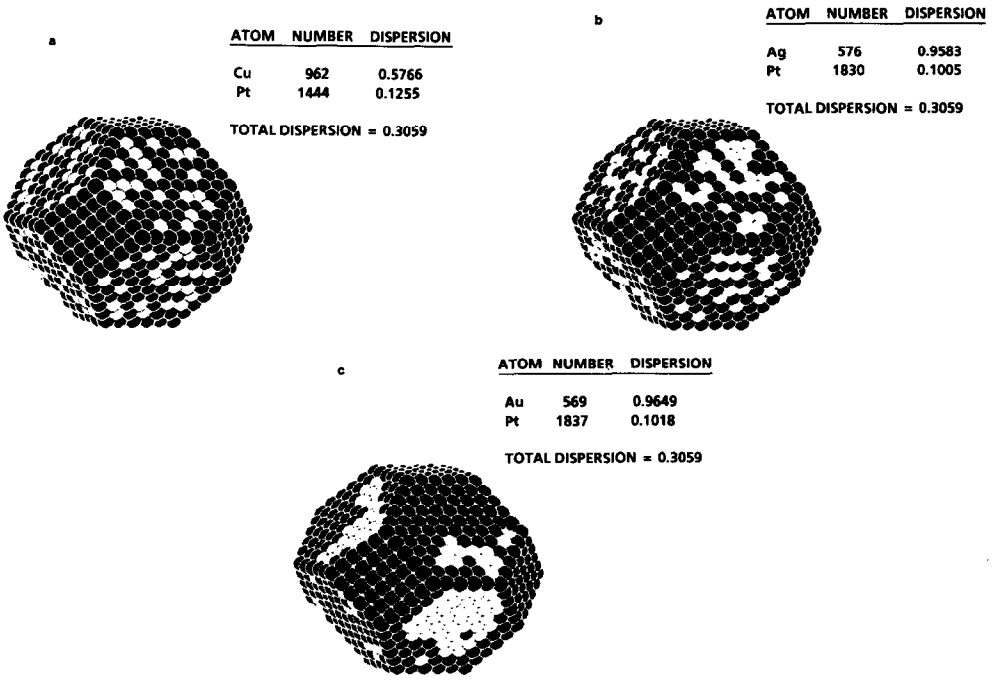

FIG. 4. Illustration of platinum ensemble sizes in Pt–Ib cubo-octahedral particles. In each case, 25% of the surface atoms are platinum. Light atoms represent platinum and dark atoms represent the Ib element: (a) Cu–Pt, T = 550 K; (b) Ag–Pt, T = 550 K; (c) Au–Pt, T = 550 K.

TABLE 6

Clustering Tendency of Surface Platinum Atoms for 2406-Atom Particles with 25% Surface Platinum at 550 K

Bimetallic system	Overall Pt atom fraction	Surface atom fraction of Pt	N^S_{Pt-Pt}
Cu–Pt (550 K)	0.600	0.25	1.21
Ag–Pt (550 K)	0.761	0.25	1.99
Au–Pt (550 K)	0.764	0.25	3.75
Cu–Pt (1150 K)	0.600	0.30	1.77
Ag–Pt (1150 K)	0.761	0.32	2.31
Au–Pt (1150 K)	0.764	0.30	2.95

Note. N^S_{Pt-Pt}, number of nearest-neighbor surface platinum atoms per surface platinum atom. Also shown is the effect of temperature on surface composition and clustering tendency.

Au–Pt particle surface has, on the average, over three times as many surface platinum atoms for nearest neighbors than does a platinum atom on the surface of a Cu–Pt particle. Such differences in the surface aggregation of Pt would, of course, result in dissimilar activities being observed for ensemble-sensitive reactions. For example, it is generally believed that hydrogenolysis reactions require at least two adjacent, catalytically active metal atoms (e.g., Pt) to occur. Therefore, after corner and edge sites of the particle became filled with the Ib metal, one would expect the hydrogenolysis activity of a Au–Pt catalyst to remain fairly constant as the Au content was increased up to the point of almost total coverage, while the hydrogenolysis activity of a Cu–Pt catalyst would decrease rapidly as the relative amount of Cu was increased.

Also shown in Table 6 is the effect of temperature on the computed surface composition and clustering tendency for the same particles shown in Fig. 4. The bulk compositions were chosen to give a 25% surface composition of platinum at 550 K. When the temperature is raised the surface composition changes in a direction to eliminate surface segregation. But, as indicated in Table 1, the energetic driving force is large compared to kT even at the much higher temperature. Consequently, the tendency to segregate is only marginally affected by an increase in temperature. Even on the (111) facets where the tendency to segregate is least, the energetic driving force is substantially larger than kT. The overall composition of Pt increases only from 25 to about 30% while the absolute temperature has more than doubled.

The effect of temperature on the clustering tendency, however, is significantly larger. For Cu–Pt and Ag–Pt the clustering tendency is higher at the higher temperature for two reasons: partly because of an increased surface composition of platinum at the higher temperature, and because the mixing energies are substantially smaller than the configurational or bond energies [see Eq. (7)]. The effect of mixing is usually at least an order of magnitude less than the pure component configurational energy. The higher temperature forces the mixing to be more random because the w/z term in Eq. (7) is on the order of or less than kT. This effect is especially notable in the case of Au–Pt where even though the platinum surface composition has increased at the higher temperature (from 25 to 30%), the clustering tendency has decreased. The number of platinum nearest neighbors in the surface for every platinum atom decreases from 3.75 to 2.95. The above results generally hold for all strongly segregating systems. The effect of temperature on surface composition is relatively small, but its effect on the clustering tendency and ensemble size can be much larger.

Monte Carlo simulations were also performed on particles that had other than perfect cubo-octahedral structure initially. Specifically, 201- and 586-atom particles with 25% Ib content were modeled and the resulting data compared to that of the cubo-octahedral catalyst particles. As discussed under Methods, these particles were simulated by assuming an initial configuration of atoms in the form of a rectangular block (the final outcome of the simulation was not significantly affected by assuming different initial shapes) and running the program at a high (typically 5000 to 8000 K) simulated

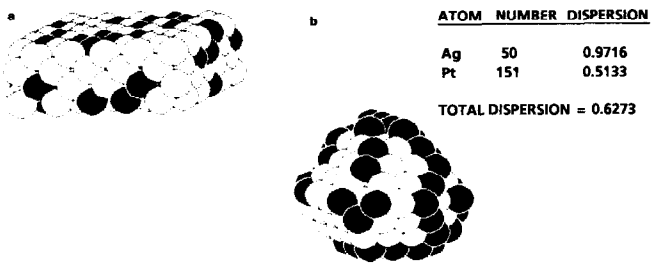

FIG. 5. Typical initial and final configurations for a 201-atom Ag–Pt particle. Dark atoms represent silver: (a) initial configuration; (b) final configuration, T = 550 K.

temperature followed by equilibration at 550 K. Typical initial and final configurations for a 201-atom particle are shown in Fig. 5. It is interesting to note that atoms initialized in a cubo-octahedral structure remained in the same structure even when heated to the same high temperatures as the atoms initialized in the block structure. This indicates the high degree of stability of the cubo-octahedral crystallite structure for FCC metals.

The results of these non-cubo-octahedral simulations are summarized in Table 7. Despite the presence of an increased amount of surface roughness (i.e.,a higher number of surface atoms with a coordination of 7 or less) on these particles, the overall surface compositions agree closely with those observed on the perfectly shaped cubo-octahedral particles. The degree of clustering of the platinum atoms on the surface of the imperfect particles (as measured by the average number of surface platinum nearest neighbors per surface platinum atom) also agrees closely with that observed on the perfectly shaped particles.

TABLE 7

Comparison of Non-cubo-octahedral Surface Coverages and Surface Platinum Nearest Neighbors per Surface Platinum Atom (N^{S}_{Pt-Pt}) to Perfectly Shaped Cubo-octahedral Particles

Bimetallic system	Particle size (No. of atoms) and initial configuration	Fractional surface coverage by Pt atoms	N^{S}_{Pt-Pt}
Au–Pt	201 c-o[a]	0.587	3.72
(25% Au)	201 b[b]	0.590	3.69
	586 c-o	0.466	3.79
	586 b	0.531	3.77
Ag–Pt	201 c-o	0.587	3.61
(25% Ag)	201 b	0.614	3.95
	586 c-o	0.470	3.51
	586 b	0.524	3.46
Cu–Pt	201 c-o	0.595	3.42
(25% Cu)	201 b	0.597	3.51
	586 c-o	0.494	3.02
	586 b	0.521	3.09

[a] Cubo-octahedral particle.
[b] Initialized in a block-type configuration.

Other simulations were performed from "block-type" initial configurations in which the number of atoms present differed from that required to form a perfect cubo-octahedral structure. Particles with 300 and 400 atoms and 25% Ib content were simulated and the resulting data compared to that of the cubo-octahedral particles in Table 8. Note that the overall surface compositions fall within the range bracketed by the cubo-octahedral particles, and the clustering of Pt atoms agrees closely with that observed on the perfectly shaped particles.

Ag–Ru Results

Table 9 illustrates several important features of the Ag–Ru system. The silver atoms segregate to the surface readily, as can be seen by comparing the overall silver content to the percentage of the surface covered by silver; they also tend to cluster. This clustering effect can be seen by noting the high fractions of silver nearest-neighbor

TABLE 8

Comparison of Surface Compositions and Surface Pt Nearest Neighbors per Surface Pt Atom (N^{S}_{Pt-Pt}) between 300 and 400 Atom Particles and 201 and 586 Atom Cubo-octahedral Particles

Bimetallic system	Particle size (No. of atoms)	Fractional surface coverage by Pt	N^{S}_{Pt-Pt}
Au–Pt	201[a]	0.587	3.72
(25% Au)	300	0.575	3.69
	400	0.564	3.59
	586[a]	0.466	3.79
Ag–Pt	201[a]	0.587	3.61
(25% Ag)	300	0.570	3.61
	400	0.549	3.61
	586[a]	0.470	3.51
Cu–Pt	201[a]	0.595	3.42
(25% Cu)	300	0.585	3.62
	400	0.559	3.47
	586[a]	0.494	3.02

[a] Cubo-octahedral particle.

atoms per silver atom. Note that in contrast to Tables 6 to 8, both bulk and surface atoms are accounted for in these fractions. In a random crystal, these fractions should, of course, be equal to the overall bulk atom fractions of silver atoms. The correspondingly high fractions of ruthenium–atom nearest neighbors per ruthenium atom can also be seen in this table.

TABLE 9

Surface Segregation and Degree of Clustering in a 2406-Atom Ag–Ru Cubo-octahedral Particle

Atomic fraction Ag	Fraction of surface covered by Ag	F_{Ag-Ag} final configuration[a]	F_{Ru-Ru} final configuration[b]
0.13	0.39	0.51	0.95
0.20	0.57	0.61	0.92
0.30	0.72	0.72	0.91
0.40	0.83	0.78	0.89
0.50	0.89	0.83	0.86

[a] Fraction of nearest-neighbor atoms to an Ag atom that are Ag atoms (average values).

[b] Fraction of nearest-neighbor atoms to a Ru Atom that are Ru atoms (average values).

TABLE 10

Comparison of Relative Ru Dispersions between Monte Carlo Predictions and Chemisorption Measurements

Atomic % Ag	$Ru^{Surface}/Ru^{Total}$	
	H_2 chemisorption	Monte Carlo[a]
0.0	0.289	0.306
0.134	0.232	0.215
0.20	0.205	0.166
0.30	0.172	0.121
0.40	0.114	0.087
0.50	0.060	0.067

[a] 2406-atom cubo-octahedral particle.

A comparison between the predicted and measured values of relative ruthenium dispersion is given in Table 10. Agreement between Monte Carlo results and hydrogen chemisorption measurements is very good throughout the range of silver content, even up to a silver to ruthenium ratio of one. This is in contrast to what was observed in the Ag–Pt system where the chemisorption results showed a higher relative group VIII (Pt) dispersion at high silver content than was predicted by the Monte Carlo technique. The better agreement could be either due to a more uniform particle size and component distribution or due to the lesser effect of chemisorption on this system because of the extremely high cohesive energy of ruthenium. Thus, it would appear that in the Ag–Ru catalysts studied, the silver atoms remained in contact with a core of ruthenium atoms and gradually covered almost the entire surface.

Pt–Rh Results

Simulations of the Pt–Rh system provided some very interesting results that are summarized in Table 11. This system is unique compared to those studied up to this point in that the element that undergoes net surface segregation does not tend to dominate the low-coordinated corner and edge sites of the crystallite. For example, in the

TABLE 11

Fraction of Lattice Sites Occupied by Rhodium Atoms in a Pt–Rh Particle (1289 Total Atoms, 0.37 Dispersion)

Overall atomic fraction Rh	Fraction surface covered by Rh	Fraction of site occupied by Rh coordination				
		6	7	8	9	12
0.50	0.27	0.88	0.56	0.21	0.12	0.64
0.65	0.40	0.95	0.78	0.41	0.22	0.80
0.65 (1450 K)	0.47	0.89	0.76	0.46	0.33	0.76
0.75	0.52	0.98	0.90	0.52	0.34	0.89
0.90	0.79	0.98	0.97	0.80	0.70	0.97

Note. Temperature is 973 K unless indicated otherwise.

case of a particle containing 65% rhodium, it can be seen that 40% of the surface will be covered by rhodium atoms, yet the rhodium atoms dominate the 6- and 7-coordinated sites with the platinum atoms preferring to occupy the planar surface sites. Such behavior is due primarily to the nature of the configurational energy differences arising in this system. Although the configurational energy change is negative for a situation in which a bulk platinum atom is exchanged with a surface rhodium atom having a coordination of 7, 8, or 9, the configurational energy change is actually positive for an exchange between a 6-coordinated rhodium with a fully coordinated platinum atom. Furthermore, even though an edge platinum atom is "preferred" over a bulk platinum atom, there is a very strong configurational energy driving force that tends to switch an edge platinum atom with a planar (8- or 9-coordinated) rhodium atom. The effect of temperature on the Pt–Rh system is also shown in Table 11. Again, the effect is relatively small. It is important to note that the largest effect is for the 9-coordinated (111) surface where the energetic driving force is the smallest.

Because the Rh surface free energy and heat of mixing for the Pt–Rh system were estimated, the reader should be cautioned that the simulation results necessarily reflect that fact. Nevertheless, it is helpful to know that the behavior observed in this system is easily within the realm of possibility.

CONCLUSIONS

The Monte Carlo simulation technique, when used with the surface-modified pair potential model, can provide useful insights into the surface composition and geometry of bimetallic catalysts. As with any modeling technique, one must constantly be aware of its assumptions and limitations. The data presented in this work were obtained from single particle simulations, assuming perfectly shaped cubo-octahedral initial structures for the majority of cases. In an actual bimetallic catalyst, however, one is dealing with particles that have a wide range of sizes, shapes, and compositions. The manner in which these bimetallic particles are distributed among these characteristics directly affects the observed properties of the catalyst. One must, therefore, consider these facts before trying to correlate simulation results with experimental data. Taken in the proper context, however, the general simulation results regarding particle sizes, surface segregation, and ensembling behavior can provide useful guidelines in designing bimetallic catalysts and in interpreting their behavior.

ACKNOWLEDGMENTS

The authors thank Xi Wu for supplying the catalysts used in the experiments and for his assistance in performing chemisorption measurements. This material is based upon work supported by the National Science Foundation under Grant CPE-8307959. The support of the Engineering Research Institute at Iowa State University is also acknowledged.

REFERENCES

1. Sinfelt, J. H., Lam, Y. L., Cusumano, J. A., and Barnett, A. E., *J. Catal.* **42,** 227 (1976).
2. Sinfelt, J. H., "Bimetallic Catalysts." Wiley, New York, 1983.
3. Sinfelt, J. H., Barnett, A. E., and Carter, J. L., U.S. Patent, 3,617,518 (1971).

4. Jacobson, R. L., Kluksdahl, H. E., McCoy, C. S., and Davis, R. W., *Proc. Amer. Pet. Inst. Div. Refin.* **49,** 504 (1969).
5. Datye, A. K., and Schwank, J., *J. Catal.* **93,** 256 (1985).
6. Galvagno, S., Schwank, J., Parravano, G., Garbassi, F., Marzi, A., and Tauszik, G. R., *J. Catal.* **69,** 283 (1981).
7. Iglesia, I., and Boudart, M., *J. Catal.* **81,** 204 (1983).
8. Masao, M., Ashida, K., Takayasu, O., and Takeuchi, T., *J. Catal.* **102,** 309 (1986).
9. Burton, J. J., Hyman, E., and Fedak, D. G., *J. Catal.* **37,** 106 (1975).
10. Tsai, N., Abraham, F. F., and Pound, G. M., *Surf. Sci.* **77,** 465 (1978).
11. Sundram, V. S., and Wynblatt, P., *Surf. Sci.* **52,** 569 (1975).
12. Metropolis, N., Rosenbluth, A. W., Rosenbluth, M. N., Teller, A. H., and Teller, E. J., *Chem. Phys.* **21,** 1087 (1953).
13. Donnelly, R. G., and King, T. S., *Surf. Sci.* **74,** 89 (1978).
14. King, T. S., and Donnelly, R. G., *Surf. Sci.* **141,** 417 (1984).
15. Foiles, S. M., *Phys. Rev. B* **32**(12), 7685 (1985).
16. Schwoebel, R. L., *J. Appl. Phys.* **38,** 3154 (1967).
17. Hultgren, R., Desai, P. D., Hawkins, D. T., Gleiser, M., Kelley, K. K., and Wagman, D. D., "Selected Values of the Thermodynamic Properties of the Elements." American Society for Metals, Metals Park, OH, 1973.
18. Mukherjee, K., *Philos. Mag.* **12,** 302 (1965).
19. Tyson, W. R., *Canad. Metall. Q.* **14,** 307 (1975).
20. Murr, L. E., "Interfacial Phenomena in Metals and Alloys." Addison–Wesley, Reading, MA, 1975.
21. Guggenheim, E. A., "Mixtures," p. 38. Clarendon, Oxford, 1952.
22. Prausnitz, J. M., "Molecular Thermodynamics of Fluid-Phase Equilibria." Prentice–Hall, New York, 1969.
23. Daw, M. S., and Baskes, M. I., *Phys. Rev. Lett.* **50,** 1285 (1983).
24. Daw, M. S., and Baskes, M. I., *Phys. Rev. B* **29,** 6443 (1984).
25. Puska, M. J., Nieminen, R. M., and Manninen, M., *Phys. Rev. B* **24,** 3037 (1981).
26. Foiles, S. M., Baskes, M. I., and Daw, M. S., *Phys. Rev. B* **33,** 7983 (1986).
27. Jacobsen, K. W., Nørskov, J. K., and Puska, M. J., *Phys. Rev. B* **35,** 7423 (1987).
28. Pandey, K. C., *Phys. Rev. Lett.* **49,** 223 (1982).
29. Fu, C. L., Ohnishi, S., Wimmer, E., and Freeman, A. J., *Phys. Rev. Lett.* **53,** 675 (1984).
30. Ho, K. M., and Bohnen, K. P., *Phys. Rev. B* **32,** 3446 (1985).
31. Fu, C. L., Freeman, A. J., Wimmer, E., and Weinert, M., *Phys. Rev. Lett.* **54,** 2261 (1985).
32. Pilliar, R. M., and Nutting, J., *Philos. Mag.* **16,** 181 (1967).
33. Dominguez, J. M., and Yacaman, M. J., *J. Catal.* **64,** 213 (1980).
34. Yacaman, M. J., and Dominguez, J. M., *J. Catal.* **64,** 223 (1980).
35. Schmidt, L. D., Wang, T., and Vaquez, A., *Ultramicroscopy* **8,** 175 (1982).
36. Harris, P. J. F., *Surf. Sci.* **185,** L459 (1987).
37. Miedema, A. R., *Philips Tech. Rev.* **26**(8), 217 (1976).
38. Hultgren, R., Desai, P. D., Hawkins, D. T., Gleiser, M., and Kelley, K. K., "Selected Values of the Thermodynamic Properties of Binary Alloys." American Society for Metals, Metals Park, OH, 1973.